Resolving the discrepancy in the half-life of ^{20}F

D. P. Burdette,[1,*] M. Brodeur,[1] T. Ahn,[1] J. Allen,[1] D. W. Bardayan,[1] F. D. Becchetti,[2] D. Blankstein,[1] G. Brown,[1] B. Frentz,[1] M. R. Hall,[1] S. King,[1,3] J. J. Kolata,[1] J. Long,[1] K. T. Macon,[1] A. Nelson,[1] P. D. O'Malley,[1] C. Seymour,[1] M. Skulski,[1] S. Y. Strauss,[1] and A. A. Valverde[1]

[1]*Department of Physics, University of Notre Dame, Notre Dame, Indiana 46556, USA*

[2]*Physics Department, University of Michigan, Ann Arbor, Michigan 48109, USA*

[3]*Department of Physics, University of Surrey, GU2 7XH, United Kingdom*

(Received 7 September 2018; published 4 January 2019)

We report a new precision half-life measurement of ^{20}F, performed using the β-counting station of the University of Notre Dame's Nuclear Science Laboratory. The measured half-life of $11.0160(41)_{\text{stat}}(155)_{\text{sys}}$ s resulting from this work will help resolve the longstanding discrepancy between two earlier sets of high-precision half-life measurements.

DOI: 10.1103/PhysRevC.99.015501

I. INTRODUCTION

Precision measurements of nuclear β-decay transitions provide a low-energy method to probe intricacies of the standard model [1], which are typically studied with high-energy experiments. One example is the search for second-class currents of the weak interaction that are not included in the standard model, but could potentially exist [2]. The standard model includes left-handed vector and axial-vector currents for the weak interaction, but the nature of restricting other forms only allows for upper limits of exotic contributions to be determined [3]. Such second-class currents would take the form of scalar or tensor interactions.

One simple test to look for second-class currents is to measure ft values for relevant nuclear β decays [4]. As an example, if mirror β decays do not have identical ft values, this would indicate that the weak interaction does not respect G parity [5]. This has brought attention to specific systems in the past due to the lack of accuracy in experimental measurements required to calculate ft values. Questions arose from discrepancies in ft values of the $A = 12$ isobars ^{12}N and ^{12}B [6]. This disagreement gave incentive to measure the ft value of other isobars, such as the $A = 20$ system, and test the conserved vector current (CVC) hypothesis [7]. This required a stronger constraint of experimental quantities needed to determine ft values, such as the half-life [8]. As such, several half-life measurements of ^{20}F have been performed in the past, with increasing precision as experimental methods improved.

Prior to this work, the half-life of ^{20}F had been determined from a number of conflicting measurements, with a Birge ratio, defined by the square root of the χ squared per degree of freedom [9], of 7.85(15). A Birge ratio this far away from 1 clearly signifies that this is a series of inconsistent measurements. Previous measurements of the half-life are outlined in Table I. Measurements with a precision better than 0.1 s are also shown in Fig. 1. It should be noted that none of the four most precise results are included within the region of the Birge-ratio-inflated uncertainty band, as given by the red dashed lines on Fig. 1. The most recent measurement [10] conflicts with previous measurements of comparable precision [5,11], while agreeing with three lower-precision measurements [7,12,13]. This provides a strong incentive to repeat the measurement with a different apparatus that has different inherent systematic uncertainties. An independent measurement will help resolve discrepancies between previous high-precision results. Therefore, the half-life of ^{20}F has been measured independently at the Nuclear Science Laboratory (NSL) of the University of Notre Dame.

II. EXPERIMENTAL METHOD

A radioactive ion beam of ^{20}F was produced from (d,p) transfer reactions in inverse kinematics using a ^{19}F beam passing through a deuterium gas target. The stable fluorine was produced by a source of negative ions from cesium sputtering (SNICS) and accelerated by an FN Tandem Van de Graaff accelerator with a terminal voltage of 6.6 MV. An analyzing magnet downstream of the tandem was adjusted to select ^{19}F^{6+} at 46.0 MeV. After impinging on the gas target, the primary beam was stopped by a Faraday cup located at the entrance of the first superconducting magnet of the TwinSol radioactive-beam facility [22], which refocused the reaction products past the exit of the magnet. A second solenoid was used to further separate ^{20}F^{6+} from the other reaction products. The low energy of the primary beam was selected such that the production of additional radioactive species from the reaction of ^{19}F with the deuterium gas target was energetically forbidden. The ^{20}F lifetime was then determined using the same technique as for the ^{17}F [23], ^{25}Al [24], and ^{11}C [25] half-life measurements at the NSL; we therefore refer the reader to these publications for more explicit details on the experimental apparatus.

After the production and separation of the radioactive beam using TwinSol, ions were implanted on a foil at the NSL

*dburdett@nd.edu

TABLE I. Previous half-life measurements of ^{20}F.

Year	Half-life (s)	Ref.
1959	12.5(2.0)	[14]
1959	11.4(1.0)	[15]
1960	11.2(1)	[16]
1962	11.56(5)	[17]
1963	11.36(7)	[18]
1967	10.31(7)	[19]
1967	10.81(11)	[20]
1970	11.03(6)	[7]
1975	10.996(20)	[13]
1976	11.18(1)	[5]
1987	11.03(6)	[12]
1992	11.163(8)	[11]
1995	11.11(4)	[21]
2018	11.0011(75)	[10]

β-counting station. A thick tantalum foil was mounted on the end of a paddle that rotates between irradiating and counting positions to help reduce background. The beam was implanted on the target for a period of 33 s (∼3 half-lives) and then rotated into the counting position where it remained for 220 s (∼20 half-lives). The primary beam was deflected using a steerer upstream of the tandem during the counting phase. The β particles emitted from the decay were detected with a 1 mm plastic scintillator connected to a photomultiplier tube (PMT) via a light guide. There were a total of 57 runs with various settings, each with 10–20 cycles, resulting in about 1000 total cycles.

III. DATA ANALYSIS

The data analysis followed the well-established, widely used procedure outlined in Ref. [26], which was also used for previous half-life measurements using the β-counting station [23–25]. Data analysis was performed separately by two different group members. The analysis is presented in detail in the following sections.

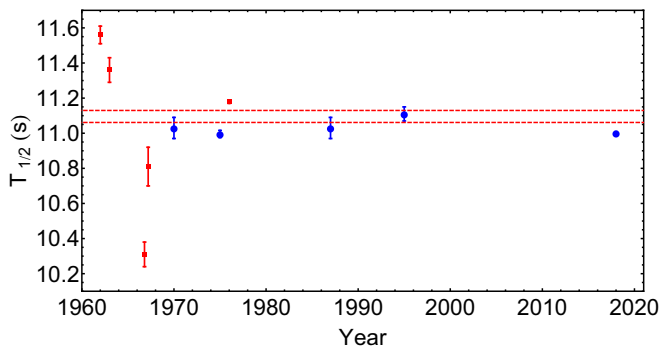

FIG. 1. All previous half-life measurements along with the Birge-ratio-inflated weighted average depicted by the dashed red lines. The color and shape of each data point indicate the fitting method used in the analysis; red squares indicate least-squares, while blue circles indicate maximum likelihood. See Sec. IV. for more details.

A. Data preselection

During the experiment, the discriminator threshold voltage, PMT voltage, and incoming beam rate were changed to probe for possible systematic biases. The data were first screened individually, on a cycle-by-cycle basis, for samples with abnormally low counts. Eight cycles, with an abnormally low number of counts, were identified as being incomplete due to premature termination of the cycle and removed from the analysis. Another test was to fit a decay curve to each cycle and observe the residuals from the fit. This method identified seven cycles with an abnormally low number of counts in the first bin affecting the residuals. This occurred when counting started while the paddle was still rotating into place.

B. Individual run sum fit

Each run consisted of 10–20 cycles with identical systematic settings. The cycles from each run were initially summed and fit individually, using the summed fit procedure prescribed in Ref. [26], to probe potential systematic biases. Prior to fitting, the data were binned into 200 bins and a correction was applied to the number of counts in each bin due to the effect of dead-time losses of the data acquisition system [26]. The decay rate was then determined for each run by fitting the following equation:

$$r(t) = r_0 \exp[-\ln(2)t/t_{1/2}] + b, \tag{1}$$

where $r(t)$ is the observed decay rate, r_0 is the initial observed rate, $t_{1/2}$ is the half-life, and b is the background rate.

Following the nature of a counting experiment, a maximum-likelihood-type fitting routine was used to fit the data. This routine iteratively fit the equation using least-squares fitting, recalculating the weight of each data point with each iteration, until it converged to fit parameters that vary by less than 0.01% from previous iterations [26].

The half-lives resulting from the fit of each individual run are shown by the data points in Fig. 2. The results are displayed as a function of the two other fit parameters: initial activity (top panel) and background (bottom panel). To gauge the statistical nature of these data, an artificial data set was created with an identical initial rate and background as the result of the fit for each run and a half-life of 11.0 seconds. The artificial data was then fit with the identical routine used for the experimental data. One hundred of those data sets were generated and fit and the 1σ confidence interval was calculated and then compared with the experimental results. This is depicted by the gray region in Fig. 2. The consistent nature of the experimental results with the 1σ confidence band from the artificial data indicate that the data follow a statistical spread.

C. Systematic subgroup sum fit

To further examine the effect of the various systematic settings used, the runs with identical settings for PMT bias and threshold voltage were added together and the fitting procedure was then repeated with each resulting summed

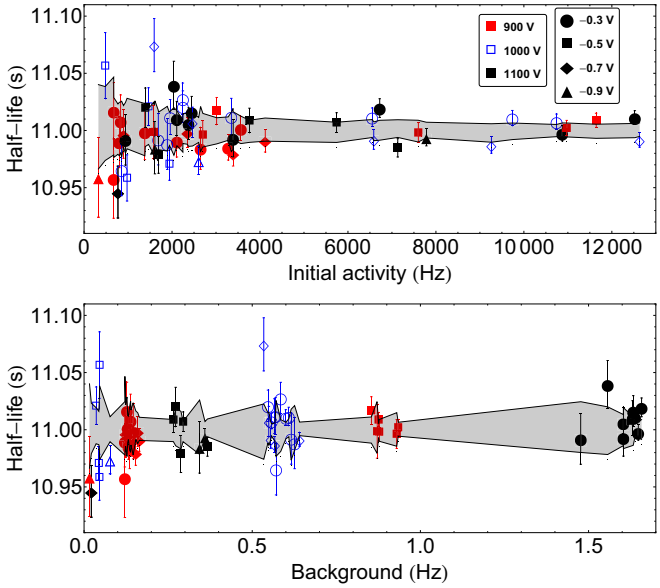

FIG. 2. The half-life, resulting from summing the cycles from each run individually, is shown as a function of the other fitting parameters; initial activity (top) and background (bottom). The color of each data point corresponds to the PMT bias used for that run, while the shape corresponds to the discriminator threshold voltage. The shaded region signifies the 1σ confidence interval resulting from the fit of 100 artificial data sets mimicking the experimental results.

data set. Once again, the procedure was replicated with 100 artificial data sets created according to the resulting fit parameters from the data. This was done to ensure there was no specific combination of settings which caused a significant change in the half-life. The results are shown in Fig 3. While a downward trend in half-life with decreasing PMT bias and discriminator threshold voltage seems to be present, it is consistent with the 1σ confidence interval of the artificial data. However, the weighted average of the 12 subgroups yield a large Birge ratio of 1.8(1), which is above the statistical ideal value of one. See Sec. III E 4 for further discussion.

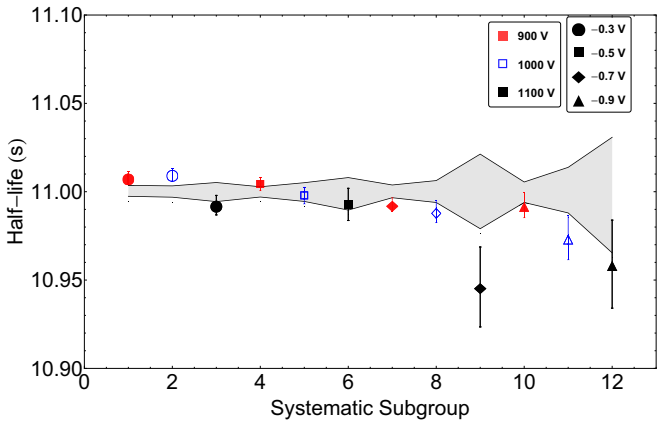

FIG. 3. Half-life results when data taken with identical systematic settings are combined. Data points along with their uncertainties indicate the result from the sum fit, while the underlaid gray region signifies 1σ confidence intervals from artificially created data.

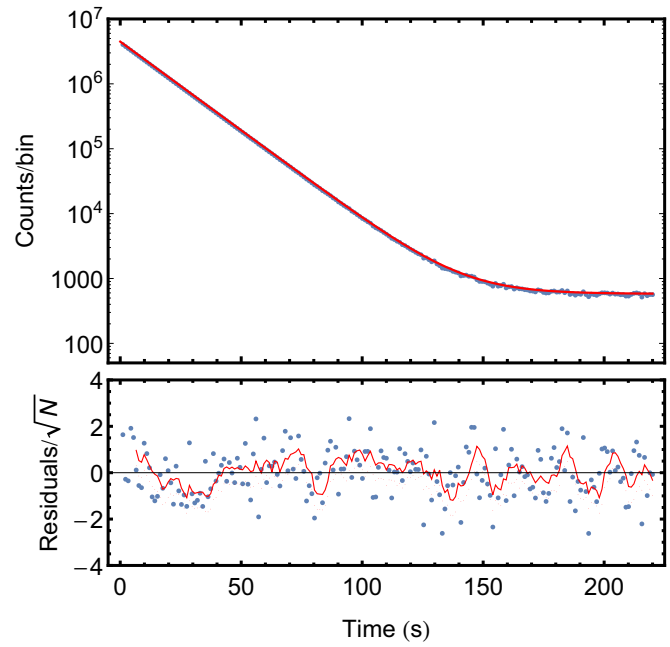

FIG. 4. The top panel shows a summed β decay curve of all cycles with the Eq. (1) fitted result shown as the red line. In the bottom panel are the residuals of the fit divided by the square root of the number of ions in a given bin N, shown as blue circles, along with a five-point moving average shown as a red solid line.

D. Sum fit

After checking the consistent nature of each subgroup of experimental settings, all cycles from each run were added together and subsequently fit with the same fitting routine. The resulting curve is given in Fig. 4.

The top panel of Fig. 4 shows the sum of the dead-time corrected data for 55 runs with the corresponding fit while the bottom panel gives the normalized residuals. The fit results in a ^{20}F half-life of 11.0006(15) s, has a reduced $\chi^2 = 0.99$, statistical spread of the residuals about a mean of 0.037, and a standard deviation of 1.003. As the residuals of Fig. 4 indicates, there exists an upward trend at the start of the decay curve that warrants further investigation. One possibility is the presence of unexpected radioactive contaminant. Hence, we performed a fit with an added unknown contaminant to the decay curve in the form

$$r(t) = r_0\{\exp[-\ln(2)t/t_1] + \alpha\exp[-\ln(2)t/t_2]\} + b, \qquad (2)$$

where α is the ratio of detected rate for the contaminant and ^{20}F, and t_1 and t_2 are the half-lives of ^{20}F and the contaminant respectively. A fitting on the sum of the same 55 runs yield a contaminant half-life of 7(3) s and an abundance ratio of 0.0056(76). Different possibilities for producing contaminants through transfer reactions in the production cell as well as fusion-evaporation reactions with possible contaminant gas in the cell, in the cell titanium windows and in the aluminum support of the implantation foil were investigated. The only

possible contaminant found with a half-life near the fitted value is ^{16}N, which has a half-life of 7.13(2) s [27].

While the primary beam energy and nuclear reaction used to produce ^{20}F for this experiment were chosen such that the production of radioactive contamination is energetically forbidden at the center of the cell, a small amount of ^{16}N might have been produced near the entrance window of the gas target. Stopping and range of ions in matter (SRIM) [28] calculations have indicated that the energy of the primary beam once leaving the 4 μm Ti foil will be 36.3(1) MeV with an energy straggling of 0.2 MeV FWHM, which is below the 39.1 MeV energy threshold to produce ^{16}N. However, if we consider the 25% lower bound in the manufacturing tolerance of the foil from the manufacturer GoodFellow, the beam energy entering the gas could be as large as 38.8 MeV with an energy straggling of 0.2 MeV FWHM, which is at the threshold to produce ^{16}N. The SRIM calculations also revealed that the primary beam undergoes a spreading of approximately 0.6 degrees FWHM as it passes through the entrance window. Once we add this to the results of a separate three-body reaction kinematics calculation that indicated that all the ^{16}N produced would be emitted at an angle of less than 1.3 degrees, it is possible that a fraction of ^{16}N has made it through the acceptance angle of TwinSol (between 1.7 and 4.5 degrees).

Since there are indications that there could have been a ^{16}N contaminant present, we fitted the first 55 runs with a contaminant fixed at the half-life of ^{16}N, 7.13(2) s, while letting the amount of contaminant vary. The resulting ^{20}F half-life is 11.0144(44) s, the contamination ratio $\alpha = 0.0056(17)$ and the reduced $\chi^2 = 0.94$ has also improved. Figure 5 shows the decay curve fitted with the ^{16}N contaminant, together with the residuals, which this time are much flatter at around zero.

A majority of the runs (55 of 57 shown in Fig. 4) had identical time durations, which when summed together result in the half-life of 11.0144(44) s. The first two cycles taken had a different duration and number of bins, which required them to be summed and fit separately. Since the amount of statistics was too low for these two cycles to get a meaningful fit with a floating α, we held it fixed at the value $\alpha = 0.0056$ found for the other 55 cycles, resulting in a ^{20}F half-life of 11.0258(107) s. The weighted average of the two data sets result in a half-life of 11.0160(41) s.

E. Systematic uncertainty estimation

Various sources of uncertainty were investigated: the uncertainty in the dead-time determination, inaccuracy in the clock time, the statistical difference in results between the fitting of various subsets of data, and the presence of contamination in the ^{20}F beam. This resulted in a total systematic uncertainty of 15.5 ms, as outlined in Table II. These sources are described in detail in the following sections.

1. Contamination

In the previous section, the presence of a ^{16}N contaminant was found to better match the observed decay curve. Naturally, there could have been other reactions with contaminants in the gas or in the windows, which might produce a radioactive contaminant that could affect a half-life measurement at this level of precision. The possibility of having such contamination was then investigated by fitting a third component to the decay curve of Eq. (2). No sign of a second contaminant, either shorter- or longer-lived was found. Furthermore, the possibility of a very-long-lived contaminant has also been studied by fitting a linear component to the decay curve of Eq. (2), yielding a slope consistent with zero.

Then, we performed a so-called channel-removal analysis, where initial sections of the decay curve are progressively removed and each time the remaining data are fitted. In the absence of contamination, a plot of the half-life as function

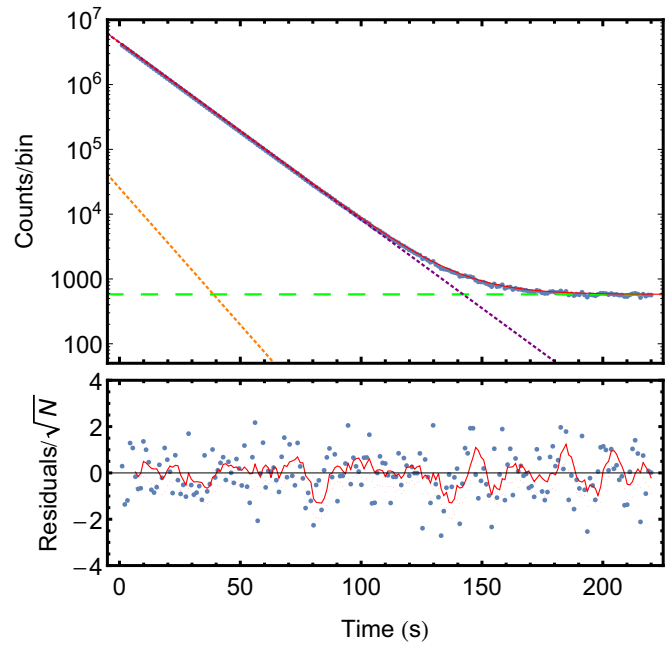

FIG. 5. The top panel shows a summed β-decay curve of all cycles with the Eq. (2) fitted result shown in red (solid). The fit includes the influence of the less abundant ^{16}N as a contaminant in orange (high-density dashing), the background in green (low-density dashing), and ^{20}F in purple (high-density dashing). In the bottom panel are the residuals of the fit divided by the square root of the number of ions in a given bin N, shown as blue circles, along with a five-point moving average shown as the red solid line.

TABLE II. Sources of systematic uncertainty on the ^{20}F half-life measurement listed in descending order of influence.

Source	Uncertainty (ms)
Contamination	15.4
Dead time	1.2
Sum fit vs. subgroup fit	1.1
Binning	0.3
^{16}N half- life	0.1
Clock time	0.1
Fitting routine	$<10^{-3}$
Total Systematic Uncertainty	15.5

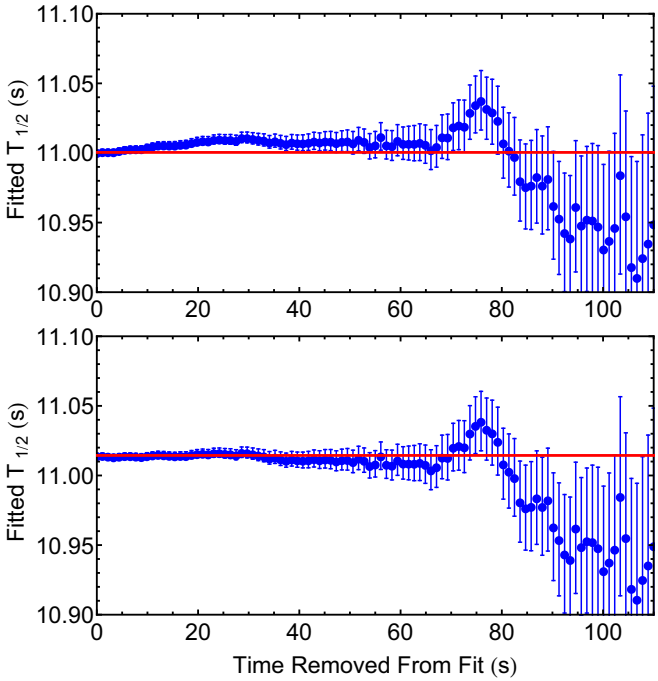

FIG. 6. Fitted half-lives for the summed data set as a function of the time removed at the beginning of the sample. The top panel gives results when fit without a contaminant using Eq. (1), while the bottom panel shows results using Eq. (2) which includes the influence of ^{16}N. Up to ten half-lives were removed.

of the time removed from the start of the decay should not present a systematic upward trend, but rather oscillate about the half-life resulting from zero bins removed. The top panel of Fig. 6, which is a channel removal applied on the summed fit without the ^{16}N contaminant fitted, shows an effect consistent with the presence of a short-lived contaminant in the measurement. This can be seen by the initial steady increase in half-life followed by its plateauing as bins are being removed. The bottom panel of Fig. 6, which includes the ^{16}N contaminant in the fit, on the other hand, shows that the fitted half-life oscillates around its original value as channels are removed.

The statistical significance of the changes in half-life with the number of bins removed has been investigated further by calculating a M-metric value as first introduced in Ref. [29], defined as:

$$M = \sum_{x=1}^{11} \mathrm{sgn}[T_{1/2}(x) - T_{1/2}(0)] \left[\frac{T_{1/2}(x) - T_{1/2}(0)}{\sigma_x} \right]^2, \quad (3)$$

where x is the number of leading channels removed, sgn is the signum function, and σ_x is the statistical error associated with the fit after removing x channels of 1 s duration. This metric helps to explore rate-dependent and diffusive systematic effects for highly correlated data [29] such as the results from the channel removal analysis. The M metric for the experimental results obtained if no ^{16}N is included is 16.9, while the metric goes down to -0.46 once ^{16}N is included. To compare these results to a Monte Carlo distribution, a

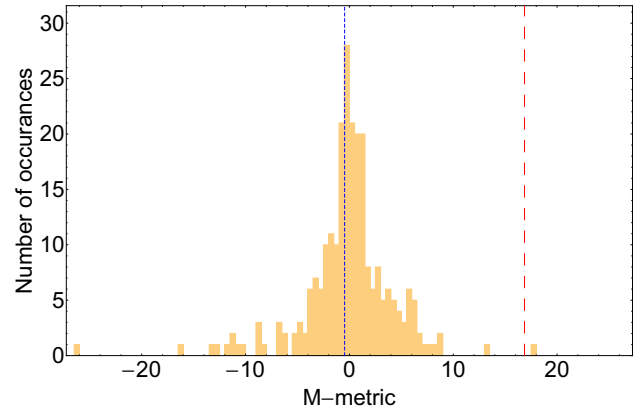

FIG. 7. M metric as defined by [29] for Monte Carlo generated data shown in yellow. This results from 250 calculations of 968 cycles mimicking the experimental data. The experimental result without consideration of a contaminant, 16.9, is given by the red dashed line. This represents the nonconsistent nature of the data in Fig. 6 with a sample absent of contamination, while the addition of ^{16}N to the decay rate reduces the value to -0.46 as shown by the blue line with denser dashing.

M metric was calculated for 250 calculations of 968 cycles (total number of cycles that passed data preselection) with the average initial count rate (4057 Hz) and background (0.55 Hz) seen in the experiment. Figure 7 shows that less than 1% of the time we get a M metric with an absolute value that is greater or equal to the experimental M metric of 16.9, while -0.46 falls in the bulk of the distribution. Hence, this is one more indication that ^{16}N contamination could be present with no other apparent contaminant.

Since the presence of ^{16}N has been inferred in the data analysis but cannot be confirmed independently, to be conservative, an additional systematic error of 15.4 ms corresponding to the difference between the sum fits without ^{16}N, 11.0006 s, and with ^{16}N was added. Also, the effect of the 20 ms uncertainty on the ^{16}N half-life on the fitted ^{20}F half-life was studied by performing fits with $t_2 = 7.11$ s and 7.15 s and we took half the difference in the ^{20}F half-life, 0.1 ms, as systematic uncertainty.

2. Dead time

The uncertainty in the determination of the dead time, $\tau = 56.89(9)\,\mu$s, will also affect the ^{20}F half-life. Hence, as done in the previous section, sum fits with $\tau = 56.80$ and $\tau = 56.98\,\mu$s were performed. Half of the difference between the two results was taken as the systematic uncertainty. The resulting value, 1.2 ms, was added in quadrature to the other systematic uncertainties.

3. Sum fit vs. subgroup fit

In Sec. III C all 57 half-life measurements of ^{20}F have been grouped according to the PMT bias and threshold voltage used. It was found that without including a ^{16}N in the fit, a large Birge ratio of 1.8(1) is obtained. Figure 8 shows the same study but with the inclusion of a ^{16}N contaminant in the fit. By

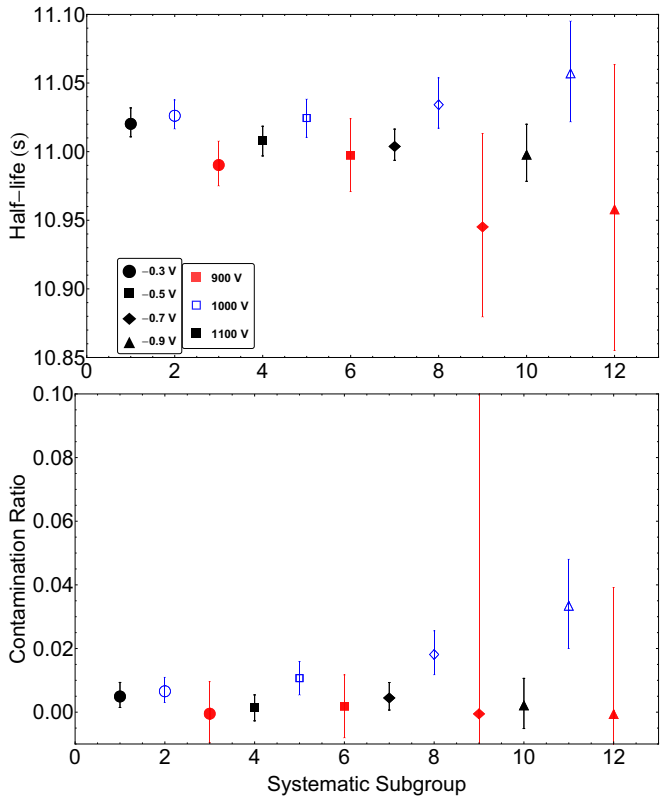

FIG. 8. Results from fitting subgroups of runs depending on the systematic settings used. The groupings are indicated by shape and color, indicating discriminator threshold voltage and PMT bias respectively. Equation (2) is used for these fits, where the contamination ratio α is floated. The top panel gives the half-life resulting from the fit while the bottom panel shows the contamination ratio.

decreasing the PMT bias and discriminator threshold voltage, the detection system becomes less sensitive to lower-energy β particles, and since ^{16}N and ^{20}F have different β-decay Q values and hence different β-decay spectral shape, α was floated separately for each subgroup. The bottom panel of Fig. 8 shows the fitted value for α while the top panel shows the fitted value for the ^{20}F half-life. As it can be seen, the fitted half-lives suffer less of a trend with decreasing PMT bias and discriminator threshold voltage. At the same time, the fitted α follow an increasing trend with decreasing PMT bias and discriminator threshold voltage. This is consistent with the higher Q value of 10.4 MeV for the β decay of ^{16}N versus the 7.0 MeV Q value for the decay of ^{20}F. Decreasing the PMT bias and the threshold voltage both results in less sensitivity at low energy, where a greater proportion of the ^{20}F β particles, as compared to ^{16}N, will fall. Hence, a large α will be seen in those cases. Finally, we took the weighted average of the 12 subgroups resulting in a half-life of 11.0149(44) s and a Birge ratio of 0.98(14).

The weighted average of the half-lives resulting from the fits of runs grouped by settings were compared to the sum fit value. The difference between these two values, 1.1 ms, was taken as a systematic contribution.

4. Binning

The effect of the choice of binning on the fitted half-life has also been tested. While we chose to fit using 200 bins for the analysis (to minimize the number of bins with zero counts in individual runs), as a systematic check we also performed fits using 500 and 1000 bins. The largest deviation from the resulting half-life came from a binning of 1000 bins. The half-lives between the two results differed by 0.3 ms, so this was also added as a small contribution to the overall uncertainty.

5. Clock time

The clock frequency has been measured using a Teledyne Lecroy 500 MHz oscilloscope to be 99.9996(10) Hz. Therefore, fits were performed with clock values determined by the upper and lower limits of the uncertainty. This resulted in a small contribution to the overall uncertainty of 0.1 ms.

6. Fitting routine

The data analysis used in the half-life determination follows a widely used method [26], as done in previous precision half-life measurements with the β-counting station. To investigate the impact of the fitting routine on the value of the half-life a second fitting routine, which minimized a χ^2 determined by Poisson statistics, was used to double check the fit [30]. The second method converged on fit parameters resulting in a χ^2 of 0.94 for the same data shown in Fig. 5. Half the difference between the two methods, 1.0×10^{-4} ms, was taken as an additional systematic uncertainty.

IV. ^{20}F HALF-LIFE

The new ^{20}F half-life measurement of $11.0160(41)_{\text{stat}}(155)_{\text{sys}}$ s is well within 1σ of the half-life value of $11.0011(69)_{\text{stat}}(30)_{\text{sys}}$ s recently published by the NSCL group [10].

We performed an evaluation of all the published half-lives and included our new measurement. Following the procedure of the Particle Data Group [31], measurements without reported error were not considered. Then, as done in previous half-life evaluations [32,33], we kept only the results with a reported uncertainty that is smaller than ten times the uncertainty of the most precise measurement. Most of the measurements excluded are pre-1960. Also, following the evaluation procedure from [33], all previous measurements using a single least-squares fit in their analysis (which is known to introduce a systematic bias in the half-life values not present in maximum-likelihood fitting) have been rejected in this evaluation of the ^{20}F half-life. These excluded results are shown in red in Fig. 1, and excluded from Fig. 9. It should be noted that two precise measurements [5,11] discrepant with the new world average by more than 13 σ have been removed. The article of the 1976 measurement [5] mentioned that a least-squares fitting procedure was used to analyze the data and a private communication with one of the authors of the 1992 measurement [11] also revealed use of the same technique [34].

The weighted average of all precise results yields a half-life of 11.0062(63) s. The Birge ratio of the world data is 1.3(2)

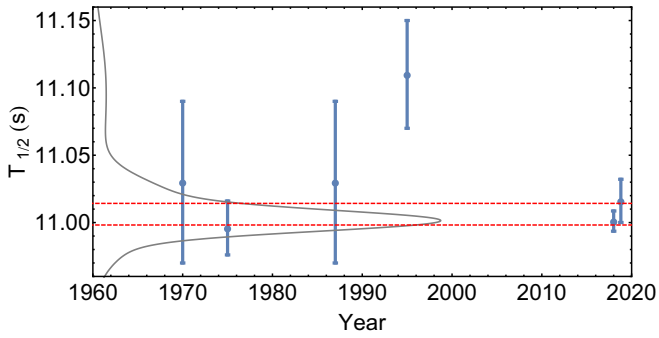

FIG. 9. ^{20}F half-life measurements considered in this evaluation [7,10,12,13,21]. The scaled uncertainty on the overall ^{20}F half-life of 11.0062(80) s is represented by the dashed red lines.

with the new measurement. Using the practices from the Particle Data Group [31], and scaling the uncertainty by the Birge ratio, gives a ^{20}F half-life value of 11.0062(80) s. Figure 9 shows all the half-life measurements considered in the evaluation together with an ideogram indicating the relative weight of each measurement. The solid gray curve shows a sum of normal distributions centered at each individual measurement with a relative height defined by σ_i^{-2} and a width of σ_i, where σ_i is the uncertainty of the measurement. The single peak of the ideogram indicates the consistent nature of the measurements used in the evaluation.

V. CONCLUSION

The longstanding discrepancy in the half-life of ^{20}F has been known for over 30 years [11]. The result from this work disagrees with two of the precision measurements from the past [5,11], while affirming the validity of the high-precision measurement reported more recently [10]. The new world average including this work is 11.0062(80) s. A consistent set of measurements has been determined by only considering results, which utilized maximum likelihood fitting.

ACKNOWLEDGMENTS

The authors would like to thank O. Naviliat-Cuncic, G. Grinyer, and G. J. Matthews for fruitful discussions. This work was supported in part by the National Science Foundation under Grants No. PHY-1713857, No. PHY-1401343, and No. PHY-1401242.

[1] N. Severijns, M. Beck, and O. Naviliat-Cuncic, Rev. Mod. Phys. **78**, 991 (2006).
[2] I. S. Towner and J. C. Hardy, in *Symmetries and Fundamental Interactions in Nuclei* (World Scientific, Singapore, 1995), pp. 183–249.
[3] D. H. Wilkinson, Eur. Phys. J. A **7**, 307 (2000).
[4] L. Grenacs, Annu. Rev. Nucl. Part. Sci. **35**, 455 (1985).
[5] H. Genz, A. Richter, B. Schmitz, and H. Behrens, Nucl. Phys. A **267**, 13 (1976).
[6] R. Blin-Stoyle and M. Rosina, Nucl. Phys. **70**, 321 (1965).
[7] D. H. Wilkinson and D. E. Alburger, Phys. Rev. Lett. **24**, 1134 (1970).
[8] N. Smirnova and C. Volpe, Nucl. Phys. A **714**, 441 (2003).
[9] R. T. Birge, Phys. Rev. **40**, 207 (1932).
[10] M. Hughes, E. A. George, O. Naviliat-Cuncic, P. A. Voytas, S. Chandavar, A. Gade, X. Huyan, S. N. Liddick, K. Minamisono, S. V. Paulauskas *et al.*, Phys. Rev. C **97**, 054328 (2018).
[11] T. Wang, R. Boyd, G. Mathews, M. Roberts, K. Sale, M. Farrell, M. Islam, and G. Kolnicki, Nucl. Phys. A **536**, 159 (1992).
[12] T. Minamisono, Hyperfine Interact. **35**, 979 (1987).
[13] D. E. Alburger and F. P. Calaprice, Phys. Rev. C **12**, 1690 (1975).
[14] S. S. Vasil'ev and L. Y. Shavtvalov, JETP **9**, 218 (1959).
[15] F. Ajzenberg-Selove and T. Lauritsen, Nucl. Phys. **11**, 1 (1959).
[16] G. Scharff-Goldhaber, A. Goodman, and M. G. Silbert, Phys. Rev. Lett. **4**, 25 (1960).
[17] S. Malmskog and J. Konijn, Nucl. Phys. **38**, 196 (1962).
[18] S. S. Glickstein and R. G. Winter, Phys. Rev. **129**, 1281 (1963).
[19] H. P. Yule, Nucl. Phys. A **94**, 442 (1967).
[20] F. Flesch and P. Hille, Oesterr. Akad. Wiss. Math–Naturw. 176, **45** (1967).
[21] S. Itoh, M. Yasuda, H. Yamamoto, K. Kawade, T. Iida, and A. Takahashi, Tech. Rep. JAERI-CONF—95-008 (1995), pp. 185–188.
[22] F. D. Becchetti, M. Y. Lee, T. W. O'Donnell, D. A. Roberts, J. J. Kolata, L. O. Lamm, G. Rogachev, V. Guimarães, P. A. DeYoung, and S. Vincent, Nucl. Instrum. Methods Phys. Res., Sect. A **505**, 377 (2003)
[23] M. Brodeur, C. Nicoloff, T. Ahn, J. Allen, D. W. Bardayan, F. D. Becchetti, Y. K. Gupta, M. R. Hall, O. Hall, J. Hu *et al.*, Phys. Rev. C **93**, 025503 (2016).
[24] J. Long, T. Ahn, J. Allen, D. W. Bardayan, F. D. Becchetti, D. Blankstein, M. Brodeur, D. Burdette, B. Frentz, M. R. Hall *et al.*, Phys. Rev. C **96**, 015502 (2017).
[25] A. A. Valverde, M. Brodeur, T. Ahn, J. Allen, D. W. Bardayan, F. D. Becchetti, D. Blankstein, G. Brown, D. P. Burdette, B. Frentz *et al.*, Phys. Rev. C **97**, 035503 (2018).
[26] V. Koslowsky, E. Hagberg, J. Hardy, G. Savard, H. Schmeing, K. Sharma, and X. Sun, Nucl. Instrum. Methods Phys. Res., Sect. A **401**, 289 (1997).
[27] D. Tilley, H. Weller, and C. Cheves, Nucl. Phys. A **564**, 1 (1993).
[28] J. F. Ziegler, M. Ziegler, and J. Biersack, Nucl. Instrum. Methods Phys. Res., Sect. B **268**, 1818 (2010).
[29] A. T. Laffoley, C. E. Svensson, C. Andreoiu, G. C. Ball, P. C. Bender, H. Bidaman, V. Bildstein, B. Blank, D. S. Cross, G. Deng *et al.*, Phys. Rev. C **92**, 025502 (2015).
[30] G. F. Grinyer, C. E. Svensson, C. Andreoiu, A. N. Andreyev, R. A. E. Austin, G. C. Ball, R. S. Chakrawarthy, P. Finlay, P. E. Garrett, G. Hackman *et al.*, Phys. Rev. C **71**, 044309 (2005).
[31] M. Tanabashi, Phys. Rev. D **98**, 030001 (2018).
[32] N. Severijns, M. Tandecki, T. Phalet, and I. S. Towner, Phys. Rev. C **78**, 055501 (2008).
[33] J. C. Hardy and I. S. Towner, Phys. Rev. C **91**, 025501 (2015).
[34] G. J. Matthews (private communication).